APL Materials

A graphene integrated highly transparent resistive switching memory device

Cite as: APL Mater. 6, 058503 (2018); https://doi.org/10.1063/1.5021099
Submitted: 01 January 2018 . Accepted: 19 March 2018 . Published Online: 30 April 2018

Sita Dugu, Shojan P. Pavunny, Tej B. Limbu, Brad R. Weiner, Gerardo Morell, and Ram S. Katiyar

A graphene integrated highly transparent resistive switching memory device

Sita Dugu,[1,2] Shojan P. Pavunny,[1,2,3,a] Tej B. Limbu,[1,2] Brad R. Weiner,[2,4] Gerardo Morell,[1,2] and Ram S. Katiyar[1,2,a]
[1]*Department of Physics, University of Puerto Rico, P.O. Box 70377, San Juan, Puerto Rico 00936-8377, USA*
[2]*Institute for Functional Nanomaterials, University of Puerto Rico, San Juan, Puerto Rico 00931, USA*
[3]*ASEE Research Fellow at U.S. Naval Research Laboratory, 4555 Overlook Ave. SW, Washington, DC 20375, USA*
[4]*Department of Chemistry, University of Puerto Rico, P.O. Box 70377, San Juan, Puerto Rico 00936-8377, USA*

(Received 1 January 2018; accepted 19 March 2018; published online 30 April 2018)

We demonstrate the hybrid fabrication process of a graphene integrated highly transparent resistive random-access memory (TRRAM) device. The indium tin oxide (ITO)/Al_2O_3/graphene nonvolatile memory device possesses a high transmittance of >82% in the visible region (370-700 nm) and exhibits stable and non-symmetrical bipolar switching characteristics with considerably low set and reset voltages (<±1 V). The vertical two-terminal device shows an excellent resistive switching behavior with a high on-off ratio of ~5×10^3. We also fabricated a ITO/Al_2O_3/Pt device and studied its switching characteristics for comparison and a better understanding of the ITO/Al_2O_3/graphene device characteristics. The conduction mechanisms in high and low resistance states were analyzed, and the observed polarity dependent resistive switching is explained based on electro-migration of oxygen ions.
https://doi.org/10.1063/1.5021099

Resistive switching is a basic physical phenomenon in which resistivity of materials can be electrically modulated between nonvolatile high and low conducting logic states. The potential incorporation of resistive random access memory (RRAM) in the realm of next generation highly scaled electronic and optoelectronic circuits and neuromorphic computing is envisaged owing to its high operation speed (~100 ps), high-density storage, low power consumption, excellent endurance (10^{12} cycles), low cost, and simple cell architecture.[1–9] Recently, extensive interest has risen in visible transparent electronic circuit applications such as integrated solar panel, touch panel, and wearable displays[10] and large-area sensors[11] in consumer electronics, defense, space, civilian, and transport sectors. Transparency of the display, logic, and memory units of the integrated circuit is essential to establish the above goal. High optical transparency and high electronic conduction are two mutually exclusive properties. Although researchers have demonstrated see-through transistors,[12,13] high transparency with efficient charge trapping is still a challenging task in mainstream floating gate thin film storage memories in addition to their physical scaling limitation. This issue can be overcome by RRAM that works on a non-charge-based mechanism[14] as long as both resistance-active (oxide) material and electrodes possess more than 80% transparency throughout the visible spectrum.[15–17] Over the past few years, considerable effort has been made to address this existing challenge by developing a variety of new material combinations that include oxides, organics, two-dimensional conductors, and nanostructures in vertical and planar sandwiched architectures and device processing techniques.[15,18–22]

[a]Authors to whom correspondence should be addressed: shojanpp@gmail.com and rkatiyar@hpcf.upr.edu. Tel.: 787 751 4210. Fax: 787 764 2571.

With the motivation to design and evaluate transparent, lightweight, and scalable devices, we have studied the switching behavior of a transparent resistive random-access memory (TRRAM) fabricated on a glass platform with semiconductor process friendly Al_2O_3 as a functional oxide layer, intensively researched graphene as a top electrode, and conventional n-type (partly due to oxygen vacancies) ITO as bottom electrodes for non-volatile memory applications. Binary oxides such as HfO_2,[23] TiO_2,[24] NiO,[25] ZrO_2,[26] Nb_2O_5,[26] and Al_2O_3[27] have been extensively studied for the fabrication of RRAM due to their simple conformation, good compatibility with CMOS back end of line technology, and low-cost of fabrication. Al_2O_3 has drawn the particular attention of scientific community because of its moderately high permittivity of ~8–10, wide optical bandgap of ~9 eV with transparency down to deep UV (beneficial for the initial high resistance state), large breakdown electric field of ~5–30 MV/cm, good thermal stability of as high as 1000 °C, and low cost.[11] Based on these properties, Al_2O_3 has found potential applications like high-k gate insulator in thin film transistors,[28] tunnel-control oxides in flash memory,[29] resistance switching layer in RRAM,[30] dielectric layer in metal/insulator/metal (MIM) capacitors,[31] surface modification at the cathode in Li-ion batteries that improves the cycle stability of the cell,[32] and gas diffusion barrier in organic electronic devices,[33] to name a few. Graphene, a two-dimensional crystal made up of just hexagonal covalent bonded carbon atoms, possesses unique electronic properties such as high charge carrier mobility (~10^4 cm^2/V s), electrical (~2000 S/cm) and thermal (~5000 W/mK) conductivities, mechanical strength (~40 N/m), and flexibility.[34–36] It is a promising candidate material for transparent conductor applications due to its low sheet resistance (~30 Ω/□) and low light absorbance (only ~2.3%)[37,38] and has the potential to replace the commercially available transparent conducting electrode, ITO, in near future. Being a good transparent conductor as well as oxygen passivation layer, graphene has shown to be an effective electrode material for various devices. For example, Yang *et al.*[10] have shown that insertion of graphene layer above the oxide layer helps in reducing resistance variation of high resistance states. Lee *et al.*[39] reported that graphene electrodes improved the performance of pentacene organic FET significantly such as minimized channel resistance, high mobility, and reduced effective barrier height compared to traditional Au electrodes. In this study, in order to figure out the efficiency of graphene as the top electrode in the device, we have compared its performance with an identical device but with conventional platinum as a top electrode.

Commercial low cost 180 nm thick ITO coated glass was used as a substrate for Al_2O_3 thin film deposition. About 15 nm thick amorphous Al_2O_3 layers were deposited on these substrates by plasma-enhanced atomic layer deposition (PE-ALD) in a Picosun R200 system at an optimized growth rate of 1.1 Å/cycle. Trimethyl aluminum (TMA) was used as a precursor of aluminum, and oxygen plasma acted as an oxidizing agent. The substrate temperature was maintained at 200 °C, a low device processing temperature. The thickness of the deposited film was measured using a JA Woollam spectroscopic ellipsometer. X-ray photoelectron spectroscopy (XPS) was performed on the Al_2O_3 layer with a monochromatized Al K_α X-ray source operating at a base pressure of 4.9×10^{-9} Torr. Monolayer graphene (G) used in the device as the top electrode was grown on copper in a hot filament chemical vapor deposition (HFCVD) reactor at a substrate temperature of 1000 °C and a filament temperature of 1600 °C by flowing 1 sccm of methane for 80 min in a hydrogen atmosphere of 35 Torr. The graphene layer was then transferred from copper to Glass-ITO/Al_2O_3 by a standard poly methyl methacrylate (PMMA) assisted wet transfer method. About 500 nm thick layer of PMMA (MicroChem 950 A9) was spin-coated on the copper/graphene sample and, subsequently, baked on a hot plate at a temperature of 150 °C for 10 min. The copper substrate was then etched out by 20% ammonium persulfate solution. The obtained G/PMMA sample was rinsed several times in de-ionized water and placed onto the ITO/Al_2O_3 sample that was placed overnight on a hot plate set at 45 °C. Finally, the top PMMA layer was removed by selectively dissolving it in hot acetone to obtain a layer of graphene on ITO/Al_2O_3. To obtain graphene as a top electrode first, we evaporated ~200 nm thick square gold layer on the 2D material through a metal shadow mask. The device was then subjected to oxygen plasma etching at a power of 80 W under a pressure of 200 mTorr to remove the graphene which was uncovered by gold. The gold layer covering the non-reacted graphene was removed by a reclamation process to obtain patterned graphene top electrodes. For this purpose, the sample was kept in a solution of 4 gm of KI, 1 gm of I_2,

and 40 ml of de-ionized water for 10 h and then dried by N_2. The gold removal can be explained by the following series of reactions.[40] $I_2 + KI \rightarrow K^+ + I_3^-$, iodine reacts with potassium iodide to form potassium ion and tri-iodide anion. These products can react with gold to form potassium auric iodide, $3K^+ + 3I_3^- + 2Au \rightarrow 2KAuI_4 + K^+ + I^-$. Hence the gold completely reacts with potassium and iodine ion leaving the ITO/Al_2O_3/G sample gold free. The device fabrication process is schematically shown in Fig. 1(a).

The surface topography of the graphene electrodes and active oxide layer was analyzed in vacuum using a scanning electron microscope operating at 70× magnification. Phase purity of processed graphene was further confirmed by Raman spectroscopy. The laser line at 514.5 nm from a Coherent argon ion laser (Innova 70-C) was focused on the sample. A liquid nitrogen-cooled CCD device collected the Raman scattered signal through a 50× objective. The transmittance spectra of the device were recorded by a ratio recording, computer controlled UV-visible spectrometer (Shimadzu UV-2450) in the spectral range of 280–800 nm. I-V measurements were done at room temperature using a Keithley electrometer (model #2401) with the top electrode DC biased and the bottom electrode grounded. For comparative study, ~50 nm thick and ~90 μm broad square platinum dots were deposited on an identical ITO/Al_2O_3 sample by dc-magnetron sputtering at a power density of 1 W/cm^2 using a metal shadow mask to form the ITO/Al_2O_3/Pt capacitor structure (control device) as shown in Fig. 1(e).

Figure 1(b) shows the SEM image of well-defined graphene top electrodes having an area of ~80 × 80 μm^2. The Raman spectra showed in Fig. 1(c) provided an intensity ratio of the two prominent peaks; G-band (1580 cm^{-1}) originated from the in-plane vibration of sp^2 carbon atoms and 2D-band (2689 cm^{-1}) due to the two-phonon double resonance as 0.5. This figure along with a full-width at half maximum (FWHM) of ~12 cm^{-1} for G-band and ~32 cm^{-1} for 2D-band confirmed the monolayer nature of graphene. Figure 1(d) shows that the fabricated device is highly transparent in the visible region (370-700 nm) with an optical transparency of >82%. It is apparent that the transparency of the device is not significantly affected by the process of graphene electrode formation. Optical transmittance of ITO/Al_2O_3 structure is reduced slightly (only by 1.2%) because of low optical

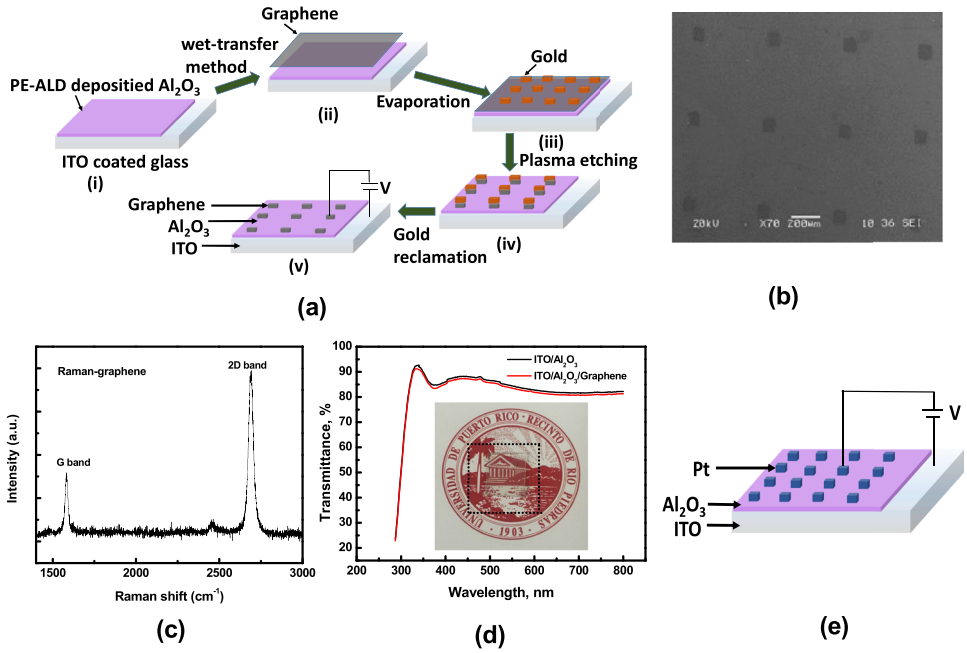

FIG. 1. (a) Fabrication process of the ITO/Al_2O_3/G device (b) SEM image of graphene square dots on the Al_2O_3 layer. (c) Raman spectra of graphene on Al_2O_3 showing G- and 2D-bands. (d) Optical transmission spectra of ITO/Al_2O_3 and ITO/Al_2O_3/G samples and the inset shows the ITO/Al_2O_3/G sample placed on the university logo. (e) Schematic of ITO/Al_2O_3/Pt capacitor.

absorbance in graphene.[37] Note that here graphene square dots serving as top electrodes occupy less area resulting in less transmittance reduction as compared to reported 2% reduction for the graphene layer.[41]

Figure 2 shows the resistive switching characteristics of the TRRAM devices with graphene and Pt as top or SET electrodes. Electroforming is the primary step and is an essential phenomenon in resistive switching to commence switching in the active material. This process is usually carried out by applying a high voltage or current compliance to the as-prepared switching device[5,42] that in turn leads to the controlled decrease in resistance. In this study, electroforming was observed at 4.8 V and 6.8 V for ITO/Al_2O_3/G and ITO/Al_2O_3/Pt devices, respectively, which was revealed by a sudden increase in current flow and are shown as insets (b) and (c) in Fig. 2. To avoid any electric breakdown due to high current flow, compliance current I_{cc} was set at 1 mA in both cases. In the case of ITO/Al_2O_3/G, the device turned to low resistance state (LRS), also called ON-state with a resistance of ~330 Ω (read at 0.1 V) after electroforming. On applying a negative bias voltage, the current suddenly decreased from ~1.55 mA to ~2.1 μA at ~−0.65 V, turning the device from LRS to HRS (High Resistance State) also called OFF-state, and the process is called the "RESET" process. Subsequently, applying the positive voltage bias from 0 V onwards, a rapid increase in current was observed at ~0.8 V, switching the device back to LRS again. This switching from HRS to LRS is called the "SET" process. Hence, the device is found to switch with alternate polarity and is called bipolar switching. In the case of the ITO/Al_2O_3/Pt device, SET and RESET voltages were observed at 2.6 V and −2.4 V (a drop in RESET or operation current from ~18.9 mA to ~89 μA), respectively, which is higher than the corresponding figures obtained for ITO/Al_2O_3/G.

Endurance and retention properties were measured for a better evaluation of the reliability and functional characteristics of the devices. Resistance at the ON-state is denoted by R_{ON} measured under an I_{cc} of 1 mA and that at the OFF state is denoted by R_{OFF} (both read at +0.1 V). The endurance test of the ITO/Al_2O_3/G transparent device depicted in Fig. 3(a) demonstrates no signs of memory state deterioration. For retention tests, the resistance at the ON state was read out for 10^4 s at +0.1 V, subsequently, the device was switched to the OFF state, and the resistance was recited for 10^4 s. The ratio of R_{OFF}/R_{ON} was observed to be ~5×10^3. Replotting the I-V curve in log-log scale as shown in Fig. 3(c), the conduction mechanism in the ON state of the ITO/Al_2O_3/G device was concluded to be of Ohmic nature as the slope of the plot was determined to be ~1. This can be due to the formation of conductive filaments in the device during the SET process. In the OFF state, the I-V plot showed a linear behavior at low voltages (0 to +0.4 V). However, at high voltages, the device showed a nonlinear behavior dominated by the electrode/interface-limited Schottky charge transport which can be elucidated via the room temperature linear current density (J) vs $E^{1/2}$ plot shown in the inset of Fig. 3(d). The Ohmic behavior at a lower voltage regime might be due to the remnant minor concentration of tiny conductive filaments even after rupture of majority of filaments during the SET process.

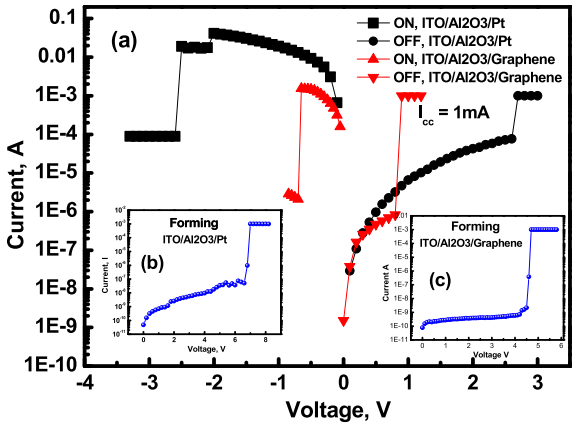

FIG. 2. (a) Resistive switching characteristics and the forming process of (b) ITO/Al_2O_3/Pt and (c) ITO/Al_2O_3/G devices.

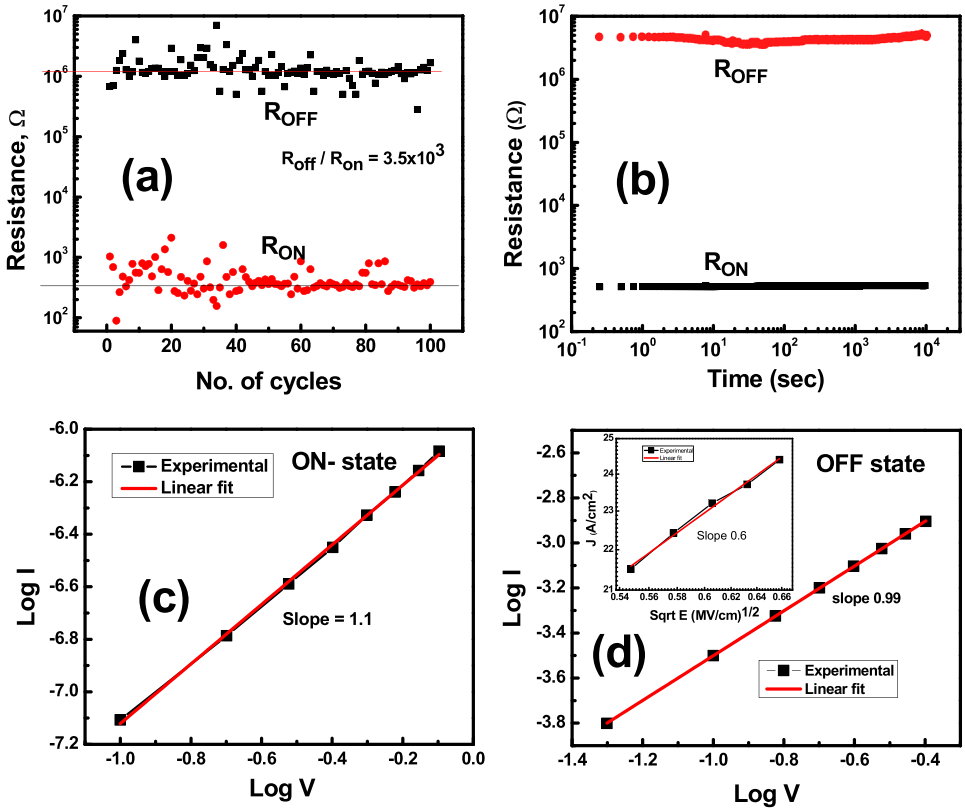

FIG. 3. (a) Endurance characteristics of the ITO/Al_2O_3/G device over 100 cycles. (b) Retention behavior of the ITO/Al_2O_3/G device over 10^4 seconds. Log-log I-V characteristics of the ITO/Al_2O_3/G device at (c) ON state and (d) OFF state. The inset of (d) shows the linear relation between J and sqrt E implying the Schottky conduction mechanism.

Endurance and retention tests conducted on the ITO/Al_2O_3/Pt device are shown in Figs. 4(a) and 4(b), respectively. The obtained R_{OFF}/R_{ON} ratio was ~10^4 and is in fairly good agreement with the study by Wu *et al.*[44] Both ON and OFF states were observed to be stable, and no significant degradation was seen. The switching ratio of approximately 10^4 in the retention of bistable resistive states may be prolonged to more than 10 years.[44] The ON state leakage curve replotted in logarithmic scale [Fig. 4(c)] can be approximated by a straight line with a slope of ~1 and confirmed Ohmic conduction. I-V characteristics for the OFF state showed a nonlinear behavior. The conduction mechanism can be identified as bulk limited Pool-Frenkel emission[44,45] as the ln J/E versus $E^{1/2}$ plot shows a linear relationship as demonstrated in Fig. 4(d). The difference between metal work-function and Fermi level of the wide bandgap semiconductor (insulator) determines the type of contact[43] during the formation of the metal-insulator interface and explains the asymmetry observed in the I-V data (Fig. 2). The work-function of graphene (~4.9 eV) and platinum (~5.2 eV) is higher than that of ITO (~4.7 eV). This higher work-function can be attributed to the formation of the Schottky barrier at the G or Pt/insulator active interface with an expected shorter barrier height for G.

The observed significant difference in SET and RESET voltages is probably the result of the electrode-oxide interaction.[41,43] Graphene shows a low sheet resistance (in-plane) and much lower contact resistance with an insulator than other conventional electrodes like Pt. G/Al_2O_3 is a Schottky contact[41] that helps us to improve the electric field intensity in the switching layer and hence a faster conductive filament growth. Also, nonpolar graphene exhibits a weak interaction with other materials resulting in an out-of-plane (6 kΩ/□) (Ref. 8) leading to a high series resistance and a low RESET current in the device. Owing to its higher work function than G, Pt is expected to have a higher Schottky barrier height with Al_2O_3 which in turn results in a larger voltage drop prior to the filament formation. The filament formation is associated with the Joule heating generated during the

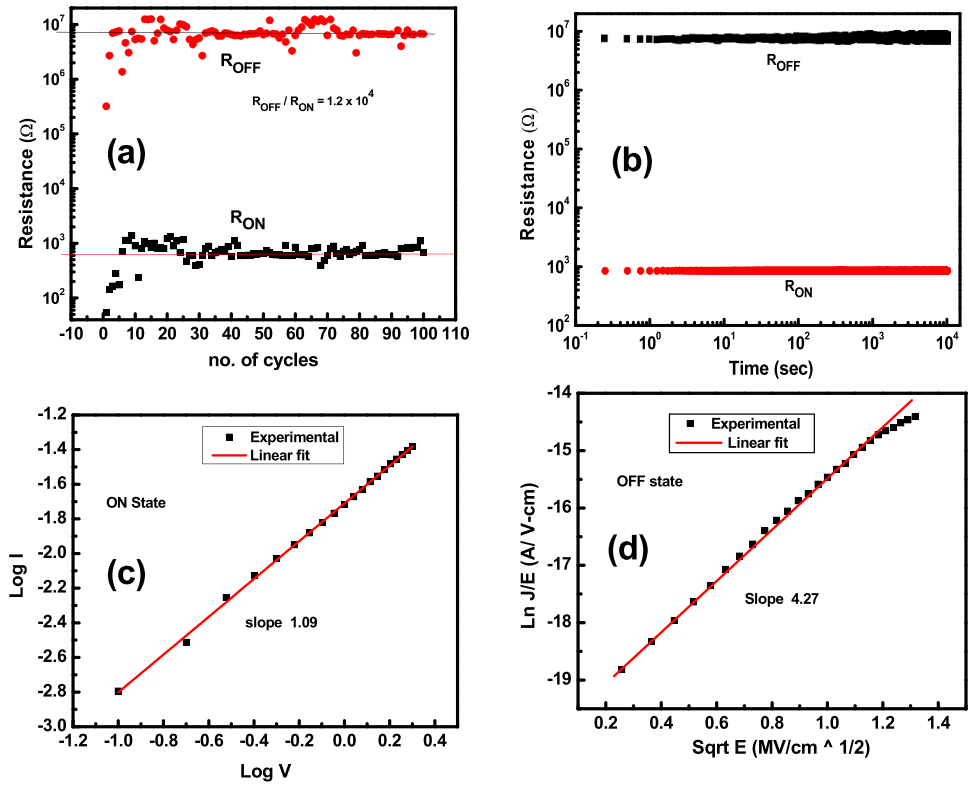

FIG. 4. (a) Endurance characteristics of the ITO/Al_2O_3/Pt device over 100 cycles. (b) Its retention behavior over 10^4 seconds. (c) Log-log I-V characteristics of the ITO/Al_2O_3/Pt device at the ON state. (d) ln J/E vs Sqrt E relation at the OFF state of the device.

Forming/SET/RESET processes.[46] The inert and atomically thin graphene has a much lower out-of-plane thermal conductivity (~6 $Wm^{-1}K^{-1}$) than its in-plane counterpart (2000-4000 $Wm^{-1}K^{-1}$)[47] and can act as an interfacial thermal resistance that can considerably reduce the heat dissipated making the programming processes more energy-efficient.[48] It can be noted that the programming power given by the product of RESET voltage and the peak in RESET current was ~1 mW for the graphene electroded device which is only ~2% of that consumed by the Pt electroded device. This indicates the possibility of reducing the programming power further by lowering the SET current compliance in scaled devices without compromising the stability in switching. Additionally, it has been proved that graphene can remove an undesired surface effect better that increases switching yield of the RRAM device.[10,41] However, a detailed study is yet to be done in this direction.

Though not well understood, various models have been proposed to illustrate the mechanism of resistive switching, such as trap charging and discharging,[49] formation and rupture of conduction filaments,[50] and modulation of Schottky barrier.[51] Several studies on metal-oxide based RRAM have shown that the generation and recombination of oxygen vacancies are responsible for switching.[22,52–54] In most dielectric layers, oxygen vacancy is the common defect which is responsible for switching. From an analysis of XPS survey spectrum shown in Fig. 5(a), the elemental ratio of Al:O:C (here C represents carbon in graphene electrode) was determined to be 0.265:0.257:0.477. An asymmetric O 1s core level spectrum [Fig. 5(b)] obtained was Gaussian deconvoluted into two peaks after Shirley background correction. The binding energy of 530.4 eV (FWHM ~ 2.23 eV) could be attributed to the oxygen that was bound to Al in the Al_2O_3 lattice, while that at 531.47 eV (FWHM ~ 2.29 eV) belongs to the oxygen deficiencies (oxygen vacancies), a common defect found in the dielectric layer. Hence, we assume that oxygen vacancies play a key role in switching mechanism as explained below.

Figure 5(c) shows the schematic of the switching process mechanism that undergoes at OFF and ON states. During the SET process, under positive bias, oxygen anions were extracted from the lattice,

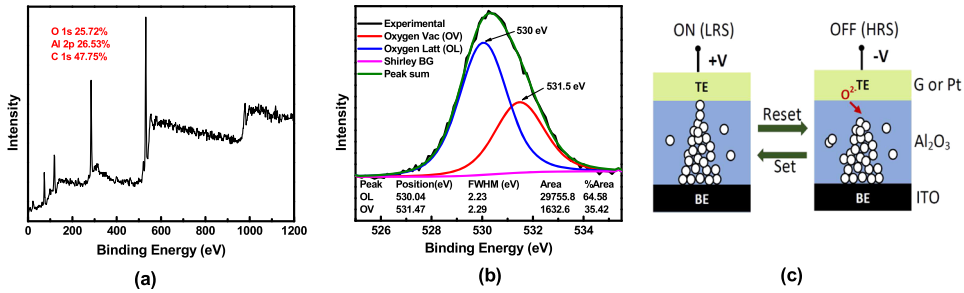

FIG. 5. (a) XPS survey spectra. (b) O 1s core level spectra of the Al_2O_3 film on the ITO substrate. (c) Schematic illustration of the RS mechanism based on the I-V characteristics.

accumulating oxygen vacancies in the disordered Al_2O_3 layer starting from the ITO/Al_2O_3 interface resulting in a considerable reduction of the Schottky barrier height at the G or Pt/Al_2O_3 interface. The Kroger-Vink notation given below expresses the formation of the oxygen vacancies,[55,56]

$$O_o \rightarrow V_o^{2+} + 2e^- + \frac{1}{2}O_2, \tag{1}$$

where O_o represents an oxygen ion in a regular site and V_o^{2+} is an oxygen vacancy with a double positive charge in the regular lattice site. Negatively charged non-lattice oxygen anions ($O^{2-} \rightarrow \frac{1}{2}O_2 + 2e^-$) thus formed are dragged toward the top electrode[57] leaving behind a more oxygen deficient Al_2O_{3-n} active layer. This process leads to the formation of a conical shaped filament made up of oxygen vacancies in the oxide layer as shown in Fig. 5(c) which acts as the low resistance path for the current flow. Hence current flows steadily through the filament resulting in a low resistance state in the Al_2O_{3-n} layer. The interface between the electrode and the oxide performs a vital role in the switching process.[57] Under the application of a negative bias voltage, non-lattice oxygen anions start to migrate from the interface, injecting into the lattice. While recombining oxygen ions with vacancies, the oxidation reaction occurs that results in a more insulating Al_2O_3 state. During this process, the conductive filaments in the Al_2O_{3-n} layer split causing a sudden drop in current. Thereafter the device gets switched to HRS and the process is called RESET.

In conclusion, we fabricated a graphene integrated see-through ITO/Al_2O_3/G TRRAM device using a hybrid process and investigated its anticlockwise bipolar resistive switching characteristics. We found that the ON/OFF resistance ratio in the ITO/Al_2O_3/G device was slightly reduced compared to that in the ITO/Al_2O_3/Pt device, but the SET/RESET voltages significantly decreased, and the RESET current was noticeably reduced which are important features for memory operations. The observed resistive switching mechanism is understood to be due to the formation and rupture of conductive filaments formed out of oxygen vacancies. Excellent endurance and retention characteristics and good contrast in the ON/OFF resistance ratio make the fabricated transparent device a potential candidate for TRRAM.

Financial support from DOD Grant No. FA9550-16-1-0295 is acknowledged. This project was supported in part by PR Space Grant (NASA Training Grant Number NNX15AI11H) and PR NASA EPSCoR (NASA Cooperative Agreement NNX15AK43A). S.P.P. thanks the American Society for Engineering Education for fellowship.

[1] Y. Y. Chen *et al.*, "Scaled x-bar TiN/HfO_2/TiN RRAM cells processed with optimized plasma enhanced atomic layer deposition (PEALD) for TiN electrode," Microelectron. Eng. **112**, 92–96 (2013).
[2] S. H. Jo *et al.*, "Nanoscale memristor device as synapse in neuromorphic systems," Nano Lett. **10**, 1297–1301 (2010).
[3] J. J. Yang, D. B. Strukov, and D. R. Stewart, "Memristive devices for computing," Nat. Nanotechnol. **8**, 13–24 (2013).
[4] A. C. Torrezan, J. P. Strachan, G. Medeiros-Ribeiro, and R. S. Williams, "Sub-nanosecond switching of a tantalum oxide memristor," Nanotechnology **22**, 485203 (2011).
[5] D.-H. Kwon *et al.*, "Atomic structure of conducting nanofilaments in TiO_2 resistive switching memory," Nat. Nanotechnol. **5**, 148–153 (2010).
[6] E. Y. Tsymbal and A. Gruverman, "Material witness: Nano contraception," Nat. Mater. **12**, 602 (2013).
[7] G. I. Meijer, "Materials Science: Who wins nonvolatile memory race?," Science **319**, 1625 (2008).
[8] S. Lee, J. Sohn, Z. Jiang, H.-Y. Chen, and H.-S. Philip Wong, "Metal oxide-resistive memory using graphene-edge electrodes," Nat. Commun. **6**, 8407 (2015).

[9] A. Pirovano and K. Schuegraf, "Integrated circuits: Memory grows up," Nat. Nanotechnol. **5**, 177–178 (2010).
[10] P. K. Yang *et al.*, "Fully transparent resistive memory employing graphene electrodes for eliminating undesired surface effects," Proc. IEEE **101**, 1732–1739 (2013).
[11] S.-W. Yeom *et al.*, "Transparent resistive switching memory using aluminum oxide on a flexible substrate," Nanotechnology **27**, 07LT01 (2016).
[12] A. Suresh, S. Novak, P. Wellenius, V. Misra, and J. F. Muth, "Transparent indium gallium zinc oxide transistor based floating gate memory with platinum nanoparticles in the gate dielectric," Appl. Phys. Lett. **94**, 123501 (2009).
[13] H. Yabuta *et al.*, "High-mobility thin-film transistor with amorphous $InGaZnO_4$ channel fabricated by room temperature rf-magnetron sputtering," Appl. Phys. Lett. **89**, 112123 (2006).
[14] R. Waser and M. Aono, "Nanoionics-based resistive switching memories," Nat. Mater. **6**, 833–840 (2007).
[15] J. Yao *et al.*, "Highly transparent nonvolatile resistive memory devices from silicon oxide and graphene," Nat. Commun. **3**, 1101 (2012).
[16] A. Sawa, "Resistive switching in transition metal oxides," Mater. Today **11**, 28–36 (2008).
[17] D. Acharyya, A. Hazra, and P. Bhattacharyya, "A journey towards reliability improvement of TiO_2 based resistive random access memory: A review," Microelectron. Reliab. **54**, 541–560 (2014).
[18] J. W. Seo, J. W. Park, K. S. Lim, J. H. Yang, and S. J. Kang, "Transparent resistive random access memory and its characteristics for nonvolatile resistive switching," Appl. Phys. Lett. **93**, 223505 (2008).
[19] J. Shang *et al.*, "Thermally stable transparent resistive random access memory based on all-oxide heterostructures," Adv. Funct. Mater. **24**, 2171–2179 (2014).
[20] J. Won Seo *et al.*, "Transparent flexible resistive random access memory fabricated at room temperature," Appl. Phys. Lett. **95**, 133508 (2009).
[21] J. Lee and O. Kim, "Nonvolatile resistive memory device based on poly(3,4-ethylenedioxythiophene):poly(styrene sulfonate) thin film for transparent and flexible applications," Jpn. J. Appl. Phys., Part 2 **50**, 06GF01 (2011).
[22] R. Waser, R. Dittmann, C. Staikov, and K. Szot, "Redox-based resistive switching memories nanoionic mechanisms, prospects, and challenges," Adv. Mater. **21**, 2632–2663 (2009).
[23] S. Lee, W.-G. Kim, S.-W. Rhee, and K. Yong, "Resistance switching behaviors of hafnium oxide films grown by MOCVD for nonvolatile memory applications," J. Electrochem. Soc. **155**, H92 (2008).
[24] B. J. Choi *et al.*, "Resistive switching mechanism of TiO_2 thin films grown by atomic-layer deposition," J. Appl. Phys. **98**, 033715 (2005).
[25] S. Seo *et al.*, "Reproducible resistance switching in polycrystalline NiO films," Appl. Phys. Lett. **85**, 5655–5657 (2004).
[26] C.-Y. Lin, C.-Y. Wu, C.-Y. Wu, T.-Y. Tseng, and C. Hu, "Modified resistive switching behavior of ZrO_2 memory films based on the interface layer formed by using Ti top electrode," J. Appl. Phys. **102**, 094101 (2007).
[27] C. Lin, C. Wu, C. Wu, C. Hu, and T. Tseng, "Bistable resistive switching in Al_2O_3 memory thin films," J. Electrochem. Soc. **154**, G189 (2007).
[28] S. Kim *et al.*, "Realization of a high mobility dual-gated graphene field-effect transistor with Al_2O_3 dielectric," Appl. Phys. Lett. **94**, 062107 (2009).
[29] S. M. Kim *et al.*, "Transparent and flexible graphene charge-trap memory," ACS Nano **6**, 7879–7884 (2012).
[30] M. Kim and K. C. Choi, "Transparent and flexible resistive random access memory based on Al_2O_3 film with multilayer electrodes," IEEE Trans. Electron Devices **64**, 3508 (2017).
[31] S. B. Chen, C. H. Lai, A. Chin, J. C. Hsieh, and J. Liu, "High-density MIM capacitors using $Al2O_3$ and AlTiOx dielectrics," IEEE Electron Device Lett. **23**, 185 (2002).
[32] L. Liu, Z. Wang, H. Li, L. Chen, and X. Huang, "Al_2O_3-coated $LiCoO_2$ as cathode material foe lithium ion batteries," Solid State Ionics **152**, 341–346 (2002).
[33] P. F. Carcia, R. S. McLean, M. H. Reilly, M. D. Groner, and S. M. George, "Ca test of Al_2O_3 gas diffusion barriers grown by atomic layer deposition on polymers," Appl. Phys. Lett. **89**, 031915 (2006).
[34] K. S. Novoselov *et al.*, "Electric field effect in atomically thin carbon films," Science **306**, 666 (2004).
[35] A. K. Geim, "Graphene: Status and prospects," Science **324**, 1530–1534 (2009).
[36] G. Jo *et al.*, "The application of graphene as electrodes in electrical and optical devices," Nanotechnology **23**, 112001 (2012).
[37] R. R. Nair *et al.*, "Fine structure constant defines visual transperency of graphene," Science **320**, 1308 (2008).
[38] J. K. Wassei and R. B. Kaner, "Graphene, a promising transparent conductor," Mater. Today **13**, 52–59 (2010).
[39] W. H. Lee *et al.*, "Transparent flexible organic transistors based on monolayer graphene electrodes on plastic," Adv. Mater. **23**, 1752–1756 (2011).
[40] R. P. Homick and H. Sloan, "Gold reclamation process," U.S. patent 3957505 (18 May 1976).
[41] X. Wang, H. Zhao, Y. Yang, and T. Ren, Graphene resistive random memory—The promising memory device in next generation, Chin. Phys. B **26**, 038501 (2017).
[42] D. Ielmini, "Resistive switching memories based on metal oxides: Mechanisms, reliability and scaling," Semicond. Sci. Technol. **31**, 063002 (2016).
[43] S. Seo *et al.*, "Electrode dependence of resistance switching in polycrystalline NiO films," Appl. Phys. Lett. **87**, 263507 (2005).
[44] S. Wu *et al.*, "Write-once-read-many-times characteristics of Pt/Al_2O_3/ITO memory devices," J. Appl. Phys. **116**, 074515 (2014).
[45] K. C. Kao, *Dielelctric Phenomena in Solids* (Elsevier Academic Press, 2004).
[46] H. Tian, H. Y. Chen, B. Gao, S. M. Yu, J. L. Liang, Y. Yang, D. Xie, J. F. Kang, T. L. Ren, Y. G. Zhang, and H. S. P. Wong, "Monitoring oxygen movement by Raman spectroscopy of resistive random access memory with a graphene-inserted electrode," Nano Lett. **13**, 651 (2013).

[47] E. Pop, V. Varshney, and A. K. Roy, "Thermal properties of graphene: Fundamentals and applications," MRS Bull. **37**, 1273 (2012).
[48] C. Ahn, S. W. Fong, Y. Kim, S. Lee, A. Sood, C. M. Neumann, M. Asheghi, K. E. Goodson, E. Pop, and H. S. Wong, "Energy-efficient phase-change memory with graphene as a thermal barrier," Nano Lett. **15**, 6809 (2015).
[49] Q. Liu *et al.*, "Resistive switching memory effect of ZrO_2 films with Zr^+ implanted," Appl. Phys. A **92**, 012117 (2008).
[50] K. M. Kim, B. J. Choi, Y. C. Shin, S. Choi, and C. S. Hwang, "Anode-interface localized filamentary mechanism in resistive switching of TiO_2 thin films," Appl. Phys. Lett. **91**, 012907 (2007).
[51] A. Sawa, T. Fujii, M. Kawasaki, and Y. Tokura, "Hysteretic current-voltage characteristics and resistance switching at a rectifying $Ti/Pr_{0.7}Ca_{0.3}MnO_3$ interface," Appl. Phys. Lett. **85**, 4073–4075 (2004).
[52] M. J. Kim, D. S. Jeon, J. H. Park, and T. G. Kim, "Bipolar resistive switching characteristics in tantalum nitride-based resistive random access memory devices," Appl. Phys. Lett. **106**, 203101 (2015).
[53] R. Mundle, H. Terry, M. Bahoura, and A. K. Pradhan, "Ozone-assisted atomic layer deposited ZnO thin films for multifunctional device applications," J. Phys. D: Appl. Phys. **46**, 475101 (2013).
[54] K. M. Kim, D. S. Jeong, and C. S. Hwang, "Nanofilamentary resistive switching in binary oxide system: A review on the present status and outlook," Nanotechnology **22**, 254002 (2011).
[55] H. Schmalzried, " F. A. Kröger: The chemistry of imperfect crystals, North-Holland Publishing Company-Amsterdam 1964. 1039 Seiten. Preis: hfl. 110,-," Ber. Bunsengesellschaft Phys. Chem. **68**, 608 (1964).
[56] D. S. Jeong, H. Schroeder, and R. Waser, "Mechanism for bipolar switching in a $Pt/TiO_2/Pt$ resistive switching cell," Phys. Rev. B **79**, 195317 (2009).
[57] Y. Du *et al.*, "The resistive switching in TiO_2 films studied by conductive atomic force microscopy and Kelvin probe force microscopy," AIP Adv. **3**, 82107 (2013).